

Hybrid Exchange–Measurement-Based Qubit Operations in Semiconductor Double-Quantum-Dot Qubits

Matthew Brooks* and Charles Tahan

Laboratory for Physical Sciences, 8050 Greenmead Dr., College Park, Maryland 20740, USA



(Received 4 June 2021; revised 6 October 2021; accepted 11 November 2021; published 8 December 2021)

Measurement-based quantum computing (MBQC) promises an alternative approach to quantum computation that has natural compatibility with error-correction codes at the cost of a polynomial increase in physical qubits. MBQC implementations have previously focused on photonic systems where two-qubit gates are difficult. On the other hand, semiconductor spin qubit systems offer fast two-qubit gates via the exchange interaction. To explore the benefits of MBQC on spin systems, two hybrid measurement-exchange schemes for full qubit control with semiconductor double-quantum-dot spin qubits are considered. Protocol 1 fully realizes the cluster-state approach to MBQC but requires singlet-triplet qubits in a magnetic field gradient. Protocol 2 implements a direct measurement-based replacement for more traditional gate-based encoded operations, without need for magnetic field gradients. Both protocols demonstrate full single- and two-qubit control through a combination of interqubit and intraqubit exchange and measurement onto the singlet-triplet basis. We show that both schemes suppress individual qubit spin-state leakage errors and offer fast gate times, up to known phase and Pauli corrections.

DOI: 10.1103/PhysRevApplied.16.064019

I. INTRODUCTION

Measurement-based quantum computing (MBQC) performs unitary rotations of encoded quantum states in a quantum processor by taking measurements, projective or partial, of qubits within entangled systems [1–7]. The amount of calculations that can be performed on a MBQC processor is limited by the amount of entangled qubits in the initial state known as the resource state. This allows for parallelization of some gates on such a processor by simultaneously performing commuting measurements of qubits within the resource state [1–11]. This is unlike more conventional quantum circuit-based models realized in solid-state systems where unitaries are achieved by driving interactions between qubits [12–15]. In such systems like superconducting circuits [13,15], trapped ions [16,17], or semiconductor quantum dots (QDs) [18–21], qubit control typically stems from interactions with externally driven electric, magnetic, or laser fields.

Semiconductor spin qubits offer long coherence times and precise control of inter-QD energy detuning and tunnel couplings [22–25] within both commercially available and isotopically purifiable semiconductors, making them excellent candidates for quantum processors. Exchange interactions allow for fast spin-spin entangling operations that are susceptible to errors due to charge noise in the controlling gates [19,26,27]. Therefore, simple encoded qubits

of two or more spins [19,28–30] are employed to protect against charge noise errors, at the cost of susceptibility to leakage errors. Leakage errors occur when the qubit couples to spin states outside the encoded qubit subspace and are generally caused by interqubit exchange interaction [31] or hyperfine interactions [32], depending on the encoded subspace. In this work we are interested in exploring MBQC with encoded spin qubits to avoid these issues by demonstrating full qubit control, within schemes that suppress qubit leakage. Such implementations are inherently compatible with error-correction schemes at the cost of a polynomial increase in the required qubits [5,33].

Typically, experimental realizations of MBQC are in photonic systems [34–36], although there has been some experimental success in trapped ion systems [37]. The challenges of photonic-based QC (lack of a two-qubit interaction) have traditionally motivated MBQC while the assumed large physical qubit resource overhead has discouraged exploration of solid-state MBQC processors. There has been some work combining photonics with QDs in cavities to build cluster states with spatially separated solid-state qubits manipulated optically [38]; however, this is dependent on preparation by measuring the random decay of the cavities, and does not levy the advantage of fast spin qubit gates with exchange. Additionally, there has been recent work in MBQC by only fermionic singlet-triplet measurement [39]; however, this method lacks analogue gate control, is not implemented in an encoded subspace, and cannot take advantage of exchange interactions.

* matthew.brooks@lps.umd.edu

A notable exception in purely solid-state implementations of quantum processors are charge parity measurement-based anyonic braiding operations in Majorana fermion qubits coupled to QDs [40–43]. This scheme however is functionally equivalent to a typical gate-based approach as there is no larger resource state employed, and thus there is less of a qubit overhead problem bar the ancilla QDs coupling the logical Majorana qubits.

Here we discuss two protocols of performing MBQC with semiconductor spin qubits assumed to be given by Si double-quantum-dot (DQD) qubits [24,44]. In the first protocol, one- and two-dimensional (2D) cluster states in spin qubits are proposed. This scheme offers efficient arbitrary single-qubit state preparation, as well as full single- and two-qubit control and compatibility with stabilizer codes by design of static qubit graph geometries. The second protocol employs entangling measurements to achieve a hybrid scheme more akin to conventional gate-based quantum computation, similar to the Majorana-qubit measurement gate schemes. Both schemes are robust against spin state leakage and offer fast gate times.

This paper is organized as follows. Firstly, the ingredients of cluster state MBQC exploited by one of our proposals are introduced in Sec. II. Then, our first hybrid exchange–MBQC control scheme is given in Sec. III, followed by the second protocol employing entangling measurements in Sec. IV. In Sec. V the methods of qubit measurement are discussed and in Sec. VI the protection of the protocols to leakage is discussed. Lastly, the results are summarized in Sec. VII.

II. CLUSTER STATES

The foundation of MBQC are quantum processors made up of large entangled states, such as a cluster state [5,33]. A cluster state $|\Psi\rangle$ is given by

$$|\Psi\rangle = \prod_{j \in N(i)} \text{CZ} |+_i\rangle \otimes |+_j\rangle, \quad (1)$$

where $N(i)$ gives all adjacent interacting qubits to qubit i , CZ gives the entangling two-qubit control-phase (CZ) gate $\text{diag}\{1, 1, 1, -1\}$, and $|\pm\rangle = (|0\rangle \pm |1\rangle)/\sqrt{2}$ are the eigenstates of the Pauli- x (σ_x) matrix. In the simplest geometry, a 1D array of qubits, each qubit is entangled with its nearest neighbor, the first of which is in some prepared state $|\psi\rangle$, with single-qubit rotations on $|\psi\rangle$ achieved by measuring each qubit along the array sequentially in the $|M_{\pm}(\theta)\rangle = (|0\rangle \pm e^{-i\theta}|1\rangle)/\sqrt{2}$ basis. Each measurement performs the rotation

$$|\tilde{\psi}\rangle = \sigma_x^s H P(\theta) |\psi\rangle = \sigma_x^s W(\theta) |\psi\rangle \quad (2)$$

on the data qubit $|\psi\rangle$, teleporting the state onto the neighboring qubit, where s is the measurement outcome [$s = 0, 1$ for $|M_{\pm}(\theta)\rangle$], H is the Hadamard gate,

and $P(\theta)$ is a phase gate, the phase of which depends on the angle of the rotated measurement basis. The σ_x^s term is a Pauli correction dependent on the measurement outcome. To perform a controlled arbitrary single-qubit rotation, a maximum of four sequential measurements accounting for the previous Pauli correction are needed since H and σ_x do not commute. Experimentally, performing an $|M_{\pm}(\theta)\rangle$ measurement is equivalent to a Pauli- x measurement $[|M_{\pm}(0)\rangle]$ between phase gates, i.e., $P(\theta) |M_{\pm}(0)\rangle \langle M_{\pm}(0)| P(-\theta)$.

Using the same tools to achieve single-qubit control, two-qubit rotations can be done in 2D arrays of cluster states. For example, a controlled-NOT (CX) gate requires only a resource state of four qubits arranged by three in a line containing the target qubit and the fourth entangled to the middle qubit as the control qubit. By two simultaneous $|M_{\pm}(0)\rangle$ measurements on the wire, the target is teleported along the wire whilst the control qubit is stationary. Therefore, if the necessary ingredients for full single-qubit control can be given for a cluster state scheme, two-qubit control can be assumed to be achievable if a 2D graph can be initialized.

III. HYBRID EXCHANGE–MEASUREMENT GRAPH PROTOCOL

A. Qubit model: magnetic gradients

In the first protocol, the qubits considered are assumed to be Si DQD spin qubits charged with two electrons, one in each dot in an $m_z = 0$ singlet-triplet $|s\rangle$ ($|t_0\rangle = (|\uparrow\downarrow\rangle \pm |\downarrow\uparrow\rangle)/\sqrt{2}$) configuration lifted from the $m_z = \pm 1$ triplet states $|t_+\rangle$ ($|t_-\rangle = |\uparrow\uparrow\rangle$ ($|\downarrow\downarrow\rangle$)) by an external magnetic B_0 field. Additionally, the qubits are assumed to experience static magnetic field gradients, implemented by micromagnets [45], or engineered g factors [46,47], across the two dots. This allows for exchange-based CZ gates to be implemented between two tunnel-coupled qubits in the limit of weak tunneling $t_{ij} \ll E_c$ (where t_{ij} is the tunnel coupling between dots i and j , E_c is the charging energy of the dots) and the exchange interaction J_{ij} between the dots satisfies $J_{ij} \ll B_0$. In this limit the exchange interaction between dots is given by $J_{ij} = 4t_{ij}^2/E_c$. This is described for two qubits coupled linearly by the exchange effective Hamiltonian (assuming that $\hbar = 1$ throughout) [31]

$$H_{\text{eff}} = (\mu \Delta_{12} + \tilde{B}) \sigma_z^1 + (\mu \Delta_{34} + \tilde{B}) \sigma_z^2 - \frac{1}{4} J_{23} (\sigma_z^1 \sigma_z^2 + \mathbb{I}), \quad (3)$$

where μ is the Bohr magneton, $\Delta_{ij} = B_i - B_j$ are the intraqubit magnetic field gradients with B_i the magnetic

field experienced by the i th dot, and \tilde{B} is given as

$$\tilde{B} = \frac{1}{2} \left[-\frac{1}{2}(\mu\Delta_{12} + \mu\Delta_{34}) + \mu\Delta_B - \sqrt{\left(\mu\Delta_B - \frac{1}{2}(\mu\Delta_{12} + \mu\Delta_{34})\right)^2 + \frac{1}{4}J_{23}^2} \right], \quad (4)$$

where Δ_B is the interqubit magnetic field difference, i.e., $\Delta_B = (B_1 + B_2 - B_3 - B_4)/2$, and σ_z^i is the Pauli- z matrix of the i th qubit in the x basis of a singlet-triplet qubit,

i.e., $\sigma_z = |0\rangle\langle 0| - |1\rangle\langle 1|$, where $|0\rangle = (|t_0\rangle + |s\rangle)/\sqrt{2} = |\uparrow\downarrow\rangle$ and $|1\rangle = (|t_0\rangle - |s\rangle)/\sqrt{2} = |\downarrow\uparrow\rangle$. Assuming QD global magnetic field gradients of $\Delta_B = \Delta_{23}$ and $\Delta_{12} = \Delta_{34} = \Delta$, and assuming that the qubits are identical and that Δ_{23} is given by the distance between adjacent qubits, a CZ gate is achieved between the two qubits when

$$\tau = \frac{\pi + 4n_1}{4\mu\Delta + 2\mu\Delta_{23} - \sqrt{J_{23}^2 + (2\mu\Delta_{23})^2}} \quad (5)$$

when the interqubit exchange satisfies

$$J_{23} = -\frac{\mu(4n_1 + 4n_2 + 1)}{4n_2(4n_1 + 2n_2 + 1)} \left[\Delta_{23} + \Delta(8n_1 + 2) + 4\Delta_{23}n_1 + \sqrt{(\Delta_{23} + 4\Delta_{23}n_1)^2 + 4\Delta^2(4n_1 + 4n_2 + 1)^2 + 4\Delta\Delta_{23}(4n_1 + 4n_2 + 1)^2} \right], \quad (6)$$

where n_1 and $n_2 \in \mathbb{Z}$. A two-qubit DQD with this geometry is depicted in Fig. 1(b). These expressions have been written with the integer constants as they demonstrate how pulse times and strengths allow for leakage to be suppressed in a gate-based regime as leakage of the qubits into spin states outside of the computational basis (i.e., $|\uparrow\downarrow\rangle$ and $|\downarrow\uparrow\rangle$) is suppressed if $J_{23} \ll \mu\Delta$ [31]. As will be evident in Sec. VI, this condition is not needed to suppress leakage in the following proposal. Alternatively, an exchange-based CZ gate can be achieved by time-crystal-inspired alternating interqubit and intraqubit exchange pulses [48]; however, this will not be considered in this work.

It can be assumed that the qubits in both proposed protocols are operated at their symmetric operating point (SOP) [26]. The SOP is the point at which $\partial E_{s/t}/\partial\epsilon = 0$, where $E_{s/t}$ are the eigenvalues of the singlet-triplet spin states and ϵ is the detuning between the two dots of the qubit. Operating here protects against first-order charge noise.

Armed with a CZ gate, the necessary ingredients for initializing a cluster state are given. Firstly, the qubits are initialized into a spin-singlet state (a $|-\rangle$ in the qubit space) by charging two electrons into one dot of each qubit and tuning the intraqubit tunnel coupling to the $(1, 1)$ charge regime, i.e., one electron per dot. Then the graph is initialized by turning on exchange interactions between the desired qubits. This encoding of the qubit space is key to exploiting fast quantum non-demolition (QND) measurement methods measuring in the singlet-triplet basis for measurement-based qubit control of the cluster state.

B. Exchange-mediated rotated measurements

Consider the following simple two DQD spin-qubit example: the first qubit in some arbitrary qubit state $|\psi\rangle = \{\cos(\theta/2), e^{i\phi} \sin(\theta/2)\}$, the second in a singlet state with exchange interaction as described by Eq. (3), again assuming identical qubits $= \Delta_{12} = \Delta_{34} = \Delta$. At some time τ the qubit initially containing $|\psi\rangle$ is measured projectively in the singlet-triplet basis, using the schemes discussed in Sec. V with outcome $s = 0, 1$ for a triplet or singlet measurement, respectively. The resulting unnormalized state in the $|0\rangle$ ($|1\rangle$) = $|\uparrow\downarrow\rangle$ ($|\downarrow\uparrow\rangle$) basis on the second qubit is

$$|\tilde{\psi}\rangle = \frac{1}{\sqrt{2}} \begin{pmatrix} 1 & (-1)^s e^{i(2\phi - J\tau)/2} \\ -e^{i(2\phi - J\tau)/2} & (-1)^{s+1} e^{2i\phi} \end{pmatrix} |\psi\rangle, \quad (7)$$

where

$$\phi = \frac{\tau(4\mu\Delta + 2\mu\Delta_{23} - \sqrt{4\mu\Delta_{23}^2 + J_{23}^2})}{2}. \quad (8)$$

Using an exchange $J_{23} = (2n + 1)\pi/\tau$ for $n \in \mathbb{Z}$, this simplifies to

$$|\tilde{\psi}\rangle = \sigma_x^{s+1} P\{(-1)^{s+1} \theta[\tau]\} W(\theta[\tau]) |\psi\rangle, \quad (9)$$

where

$$\theta[\tau] = \frac{\tau}{2} \left(4\mu\Delta + 2\mu\Delta_{23} - \sqrt{4\mu\Delta_{23}^2 + \frac{\pi^2(2n + 1)^2}{\tau^2}} \right) + \frac{(2n + 1)\pi}{2}. \quad (10)$$

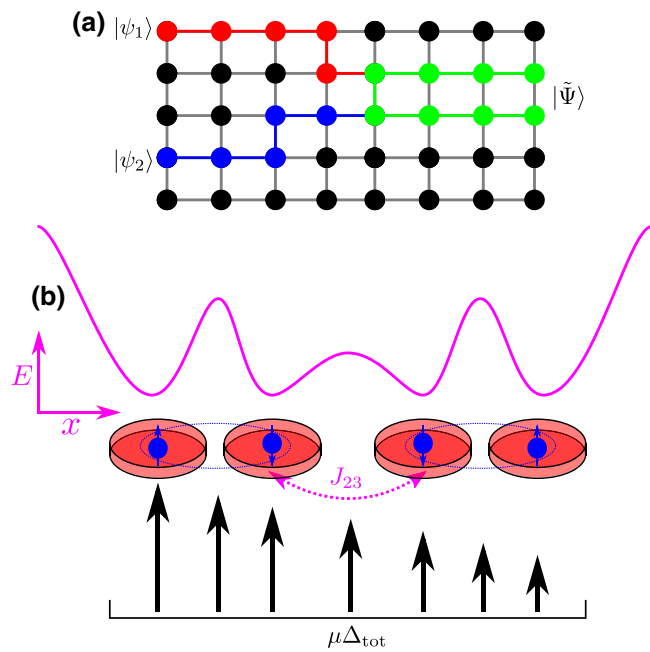


FIG. 1. (a) Grid cluster state, consisting of qubits (black dots) all initialized in the $|+\rangle$ state, entangled to their neighboring qubits by a CZ gate drawn as a black line. Two logical qubit states $|\psi_1\rangle$ (red) and $|\psi_2\rangle$ (blue) start on the left-hand side of the graph, and follow a path of measurements through the graph given by their respective color. The qubits are then entangled by a two-qubit gate measurement sequence outputting the state $|\tilde{\Psi}\rangle$, and all unused qubits in the graph can be disentangled from the output state by Pauli- z measurements. (b) Diagram of two semiconductor double-quantum-dot qubits arranged linearly. Each qubit consisting of two dots (red) is charged with one electron (blue) in an $m_z = 0$ singlet-triplet spin configuration (blue dotted line). The two adjacent dots from each qubit are coupled by an exchange interaction J_{23} (magenta dotted line) given by the depicted potential shape (magenta line). The magnetic field gradients for each qubit as well as the whole system are given (black).

The resulting projected unitary is the desired exchange-controlled single-qubit $W(\theta)$ gate, repetitions of which allow for full single-qubit control, with additional measurement-dependent phase $P[(-1)^{s+1}\theta]$ and Pauli- σ_x^{s+1} corrections. This additional phase may be corrected after the fact by intraqubit phase gates due to magnetic gradient precession. Importantly, however, the $W(\theta)$ control gate is not dependent on the measurement outcome, only the phase correction. The gate time of this projective measurement-based gate depends on the angle θ of the gate. As a benchmark, to project a Hadamard within this scheme, the gate time is approximately 20 ns [31,49], assuming measurement by curvature (discussed in Sec. V) that corrects for any leakage from the exchange interaction by projecting only onto the $m_z = 0$ subspace (discussed in Sec. VI). It is important to note here that after the

application of this protocol, the qubit that initially contained the encoded state is projected onto a state that can be immediately reused in the same protocol. This notion of reentangling spent qubits of the cluster state helps mediate the overall physical qubit cost of building a processor based on this protocol. This is explored further in Sec. III E.

C. Efficient arbitrary state preparation

Here the exchange-measurement hybrid protocols outlined in Sec. III B will be demonstrated to be useful for single measurement arbitrary state preparation. This is achieved with two qubits, assumed to both start in the spin singlet state ($|-\rangle$ in the qubit basis). The resulting teleported state after application of Eq. (9) is

$$|\psi\rangle = \begin{pmatrix} \sin[\theta/2 + \pi(2 + 2n + s)/4] \\ (-1)^{s+1}e^{i\theta} \cos[\theta/2 + \pi(2 + 2n + s)/4] \end{pmatrix}, \quad (11)$$

which can be made to be any arbitrary single-qubit state by application of a phase gate.

With this protocol, any arbitrary single-qubit state can be written with a measurement-based protocol with a single measurement. However, the state is dependent upon the measurement outcome s . The two possible states generated by the protocol are always antipodal to one another on the Bloch sphere. To recover the $s = 0$ state from a $s = 1$ measurement requires a Pauli and phase correction σ_x and appropriate phase.

D. Two-qubit gates

In a cluster state, to perform two-qubit gates, 2D graphs are necessary. With spin qubits, 2D geometries are limited in scope due to considerations such as plunger-gate placements and crosstalk. However, one of the simplest geometries, four qubits arranged in a square, can be used with the hybrid exchange-measurement graph protocol described here to perform entangling two-qubit gates. An example of this is given in Fig. 2. In this protocol, all the qubits are identical, within a global magnetic field gradient from a single micromagnet, such that the intraqubit field gradients Δ_q are identical, but the interqubit magnetic field gradients Δ_{int} depend on the alignment of the two qubits with the global magnetic field gradient. In this example, as in Fig. 2(a), horizontal Δ_{int} terms are of equal magnitude and vertical $\Delta_{\text{int}} = 0$. Initially, the two logical qubits start in the top left and bottom right of the square, and the remaining qubits in the $|+\rangle$ state. Interqubit interaction is then turned on between all neighboring qubits with time τ , at which point the qubits that previously housed the logical states are measured. The resulting states encoded in the two qubits that were not measured depend on the values of interaction strength used for each of the four interqubit exchange gates. For example, if the value of the interaction

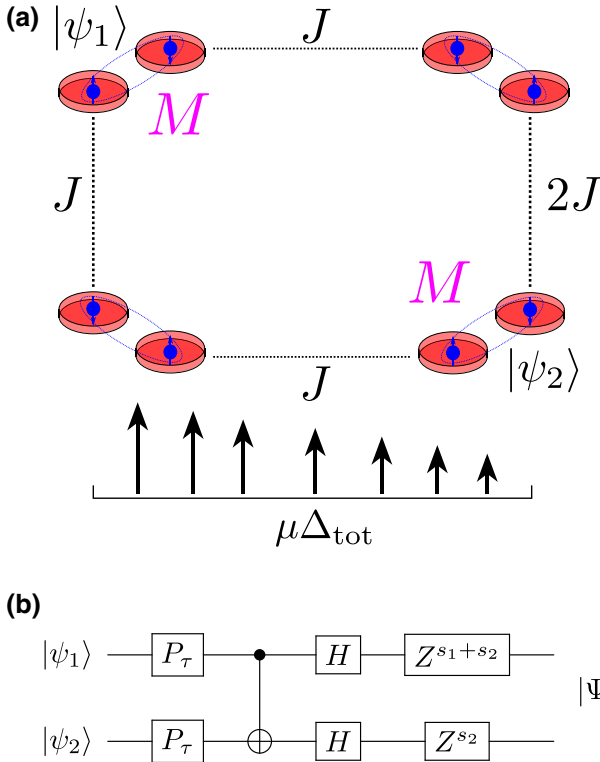


FIG. 2. (a) Four-qubit square geometry to perform an entangling two-qubit gate in the exchange-measurement hybrid cluster state protocol. The initial two qubits start in the top right and bottom left, all qubits are then entangled by exchange to their two neighbors, and singlet-triplet measurements, equivalent to projective Pauli- x measurements, are performed, resulting in an entangling two-qubit state in the remaining two qubits. (b) The equivalent gate unitary, including Pauli corrections of the exchange-measurement hybrid protocol given in (a). Here the bottom right qubit in (a) is the first logical qubit and the top left is the second. The measurement outcomes s_1 and s_2 correspond to the measurements performed on the physical qubits that initially encoded $|\psi_1\rangle$ and $|\psi_2\rangle$, respectively.

strength in Fig. 2(a) used is $J = \pi/\tau$ at times

$$\tau = \frac{\pi(n_2 + 4n_1)^2 - \pi}{-4\Delta_{\text{int}}(4n_1 + n_2)}, \quad (12)$$

where $n_1 \in \mathbb{Z}, \neq 0$ and $n_2 = 1, 5, 9, \dots$, the resulting two-qubit gate performed by this scheme is given in Fig. 2(b). Here it is also assumed that the geometry of the chip is such that the magnetic field gradients satisfy

$$\Delta_q = \frac{\Delta_{\text{int}}[4n_3(4n_1 + n_2) + 4n_1 + n_2 + 1]}{2(4n_1 + n_2 - 1)(4n_1 + n_2 + 1)}, \quad (13)$$

where $n_3 \in \mathbb{Z}$. The additional phase gates in Fig. 2(b) are $P_\tau = P\{(\pi/2)[(4n_1 + n_2)^{(-1)} + 2n_1 + n_2]\}$. Note that such a setup of magnetic field gradients and pulse times are only needed to achieve the Clifford circuit in Fig. 2(b);

this scheme gives a unitary two-qubit gate so long as three of the exchange gates satisfy $J = \pi/\tau$ and the final gate is $2J$.

E. Reentangling measured qubits

Projective measurements, like those assumed in this work, leave behind a qubit prepared in a singlet or triplet state that may be reentangled to the resource state. By again engaging the exchange interaction J_{23} , the qubit may be reentangled with the information carrying qubit to allow for repetition of a measurement-based gate on the same geometry. This circumvents the issues of resource overhead for solid-state implementations of MBQC for noncommuting measurements. The adjustments needed to do so depend upon the previous measurement result. As such, the projected gate given by protocol (9) becomes

$$|\tilde{\psi}\rangle = \sigma_z^{s_1+1} \sigma_x^{s_2} P[(-1)^{s_2}\theta] W(\theta) |\psi\rangle, \quad (14)$$

where s_1 is the result of the previous measurement performed on the qubit the state is being projected to and s_2 is the result of the current measurement projecting the state back onto the first qubit. Performing multiple gates with this protocol, the overall number of post gate corrections, i.e., up to two Pauli corrections and one phase correction, remains constant regardless of the number of iterations if the previous known anomalous phase is considered when performing the next gate. For example, as is shown in Fig. 3, assuming an initial two-qubit state $|\psi\rangle \otimes |(-1)^{s_1}\rangle$, if protocol (9) is repeated twice for two different angles θ and θ' , respectively, the applied unitary is

$$U = \sigma_x^{s_1+s_3} P[(-1)^{s_1+s_3}\theta'] W[(-1)^{s_2}(\theta' + \theta)] W(\theta). \quad (15)$$

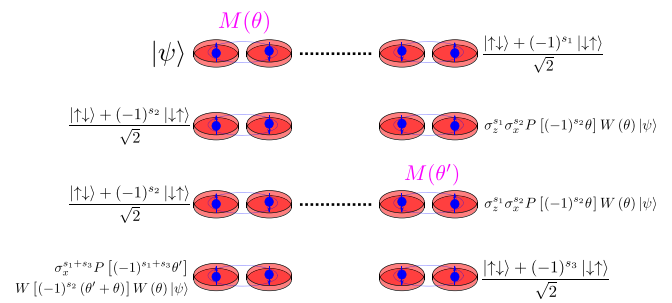


FIG. 3. Example of a simple two-qubit recycled cluster state with accumulated Pauli corrections. Initially, the left-hand qubit is prepared in some state $|\psi\rangle$ and the right-hand qubit is in either a singlet or triplet state. The protocol given in Eq. (9) is then applied to both qubits measuring the left-hand qubit, leaving it in either a singlet or triplet state and the right-hand qubit in the state given. The protocol is then applied again measuring the right-hand qubit, adjusting the rotation θ' of the second application of the protocol based on the phase correction θ of the previous iteration of the protocol.

This shows that subsequent rotations θ' may be adjusted to account for the measurement outcomes of the previous iteration of the protocol to apply the desired series of unitaries without performing a phase correction at each step. Note that if the protocol is applied an odd number of times, such as in Eq. (15), a maximum of one Pauli-x correction may be needed, whilst if the protocol is applied an even number of times, a maximum of a Pauli-x and a Pauli-z correction may be needed.

With an architecture in which each qubit can be measured and reentangled to the graph on demand, a processor that can be used both for qubit operations and quantum error-correction encoding can be designed. Graph states are naturally compatible with stabilizer codes as the stabilizers K_i of a cluster state may be inferred from its geometry as

$$K_i = (\sigma_x)_i \otimes_{j \in N(i)} (\sigma_z)_j. \quad (16)$$

For example, encoding and decoding a qubit with a $[[4, 1, 2]]$ stabilizer state has been demonstrated experimentally with a five-qubit cluster state in an optical system [50]. The graph geometry used for this code is not feasibly compatible with a spin-qubit implementation. However, a similar, linear code can be used, at the cost of distinguishing some single-qubit Pauli errors. This is achieved with an architecture of five qubits in a line. The same architecture is described in Sec. II to achieve arbitrary single-qubit rotations of the form

$$|\tilde{\psi}\rangle = W(0)W(\theta_3)W(\theta_2)W(\theta_1)|\psi\rangle \quad (17)$$

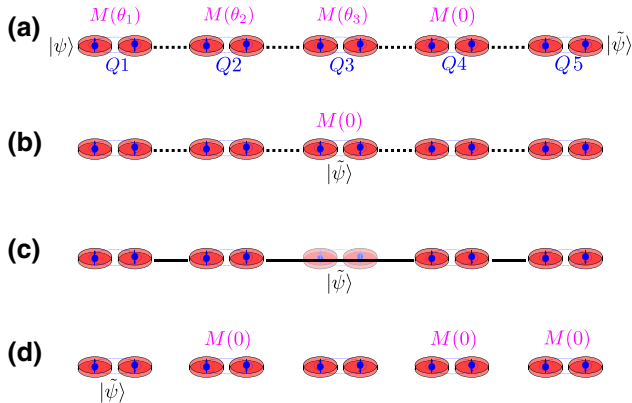


FIG. 4. (a) Linear cluster state geometry with measurements (magenta) to perform an arbitrary qubit rotation U on state $|\psi\rangle$ initially encoded in qubit $Q1$. The final state $|\tilde{\psi}\rangle = U|\psi\rangle$ is teleported to qubit $Q5$. The black dashed lines denote exchange interaction to allow for necessary measurements. (b) Graph state geometry to encode the state $|\tilde{\psi}\rangle$ to the $[[4, 1, 2]]$ stabilizer state given by the solid black lines in (c), by measuring $Q3$. (d) Protocol for decoding the stabilizer state given in (c), projected $|\tilde{\psi}\rangle$ to $Q1$.

	$\langle S_1 \rangle$	$\langle S_2 \rangle$	$\langle S_3 \rangle$	$\langle S_1 S_2 \rangle$	$\langle S_1 S_3 \rangle$	$\langle S_2 S_3 \rangle$	
Z_1	Blue	Red					
Z_2	Red	Blue					
Z_3	Red		Blue				
Z_4	Red			Blue			
X_1	Red				Blue		
X_2	Blue	Red					1
X_3		Red		Blue			-1
X_4		Red			Blue		
Y_1			Blue		Red		
Y_2		Red		Blue		Red	
Y_3	Blue						
Y_4						Blue	

FIG. 5. Table of the expectation values of the stabilizers $\{S_1, S_2, S_3\}$ and products of the linear stabilizer code given in Fig. 4 under every single-qubit Pauli on the i th error $\{X_i, Y_i, Z_i\}$. The occurrence of any single-qubit error is detectable, but some are indistinguishable from a single measurement of the syndromes.

with the rotated state ending in the fifth physical qubit. This state may then be transferred back to the middle (third) qubit by two $W(0)$ measurements. Then, by entangling all adjacent qubits with a CZ interaction and measuring the third qubit in the Pauli-x basis, $|\tilde{\psi}\rangle$ is then encoded in a $[[4, 1, 2]]$ stabilizer state across the remaining four qubits. The qubit can then be recovered to the first qubit from the stabilizer to perform additional rotations by measuring the second, fourth and fifth qubits in the Pauli-x basis. This protocol, depicted in Fig. 4, has stabilizers $\{S_1, S_2, S_3\} = \{\sigma_x \otimes \sigma_z \otimes \mathbb{I} \otimes \mathbb{I}, \sigma_z \otimes \sigma_x \otimes \sigma_x \otimes \sigma_z, \mathbb{I} \otimes \mathbb{I} \otimes \sigma_z \otimes \sigma_x\}$, and can detect any arbitrary single-qubit Pauli error, though it cannot distinguish between all such errors; see Fig. 5.

IV. ENTANGLING MEASUREMENTS PROTOCOL

The methods presented up to this point are a form of MBQC whereby the measurements provide unitary operations on the encoded qubits, at the cost of entanglement between qubits generated by exchange gates. This allows for a powerful method of processing and encoding quantum information with an at worse polynomial cost in physical qubits, which can be mediated by reentangling measured qubits. The following protocol shown here, however, implements measurements that entangle qubits, as well as measurements that rotate qubits at the cost of entanglement.

A. Qubit model: no magnetic gradients

In this scheme qubits are encoded in the Pauli-z basis of the singlet-triplet spin space $|\downarrow\rangle = (|\uparrow\downarrow\rangle - |\downarrow\uparrow\rangle)/\sqrt{2}$ and $|\uparrow\rangle = (|\uparrow\downarrow\rangle + |\downarrow\uparrow\rangle)/\sqrt{2}$ and require only controllable exchange coupling between dots within the same

qubit. No magnetic field gradients or interqubit exchange coupling are required. Therefore, the effective Hamiltonian for the interqubit and intraqubit exchange interaction of two qubits comprised of four dots [as in Fig. 1(b)] can be written as [51]

$$H_{\text{eff}} = \frac{J_{12}}{2} \sigma_z^1 + \frac{J_{34}}{2} \sigma_z^2 - \frac{J_{23}}{4} \sigma_x^1 \sigma_x^2. \quad (18)$$

Note that, since there are no magnetic field gradients considered here, if the interqubit exchange term $J_{23} > 0$, leakage to the $m_z = \pm 1$ triplet states will occur. Although this leakage will be suppressed by qubit measurement, it will be assumed that $J_{23} = 0$, as this term does not contribute to the entanglement generating steps in this protocol, the interqubit measurements.

B. Interqubit measurement

Alternatively to measuring in the basis of a logical qubit, an entangling operation can be achieved by measuring a dot from each adjacent encoded qubit, i.e., measuring in the singlet-triplet basis of the second and third QDs in Fig. 1. Forgoing any exchange interaction, the resulting two-qubit projector in the qubit basis used in Sec. III is

$$\mathcal{M} = |00\rangle\langle 00| + |11\rangle\langle 11|. \quad (19)$$

However, this measurement also entangles the encoded qubits to spin states outside of the $m_z = \pm 1$ triplet states. The measurement cannot however change the net-spin state of the two qubits it acts on and, as such, measuring either of the individual qubits in the $m_z = 0$ singlet-triplet basis corrects for the leakage, at the cost of the entanglement of the qubits.

C. Qubit control with entangling measurements

The entangling measurement described can be used along with intraqubit exchange interaction to implement an alternative noncluster state approach to MBQC. In this regime, as shown in Eq. (18), again assuming the interqubit exchange $J_{23} = 0$, the intraqubit exchange terms $J_{12(34)}$ allow for phase control in the qubit subspace. The final tool needed for single- and two-qubit control is access to an ancilla qubit initialized in the $|+\rangle = |\uparrow\downarrow\rangle$ state for each logical qubit (polynomial increase in physical qubits) and the ability to measure each qubit in the singlet-triplet basis.

With these tools, a complete set of single-qubit unitaries can be produced as follows. Suppose initially that there are two qubits, the first initialized to some arbitrary state $|\psi\rangle$ and the second in the $|+\rangle$ state. Then both qubits experience an exchange phase gate imparting phases ϕ_1 and ϕ_2 to the respective qubits, before which an entangling measurement is performed on the qubits and after which another

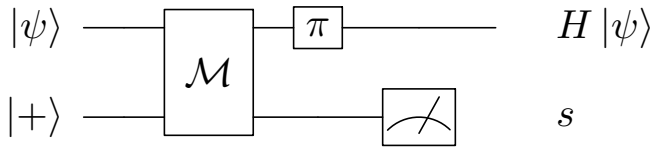


FIG. 6. Circuit diagram of the phase gates and measurement sequence needed to achieve a single-qubit Hadamard without any correction.

set of phase gates ϕ_3 and ϕ_4 are performed before the second qubit is measured with outcome s . This results in the following unitary acting on the input state in the first qubit:

$$|\tilde{\psi}\rangle = \frac{1}{\sqrt{2}} \begin{pmatrix} 1 & e^{i[\phi_1 + (-1)^s \phi_2]} \\ e^{i[(-1)^s \phi_1 + \phi_2]} & e^{i(\phi_2 + \phi_3)} \end{pmatrix} |\psi\rangle. \quad (20)$$

Then, by selecting appropriate phases, useful gates up to some known correction may be implemented. For example, Fig. 6 shows the sequence of phase gates and measurements needed to perform a Hadamard gate on the logical qubit $|\psi\rangle$ without any Pauli correction. The only measurement outcomes that determine the correction is the ancilla qubit measurement s at the end of the sequence; the entangling measurement result does not contribute. The same tools can be used to implement a two-qubit entangling gate with two ancilla qubits. The measurement and phase gate sequence needed is given in Fig. 7(a). The resulting two-qubit unitary of the sequence given in Fig. 7(a) is shown in Fig. 7(b), including the single Pauli- x correction given by the measurement results $s_1 + s_2$ of the measurement of the ancilla. This is a demonstration of implementing a Clifford gate group with the proposed scheme. This is done for simplicity to demonstrate that a universal gate set can be

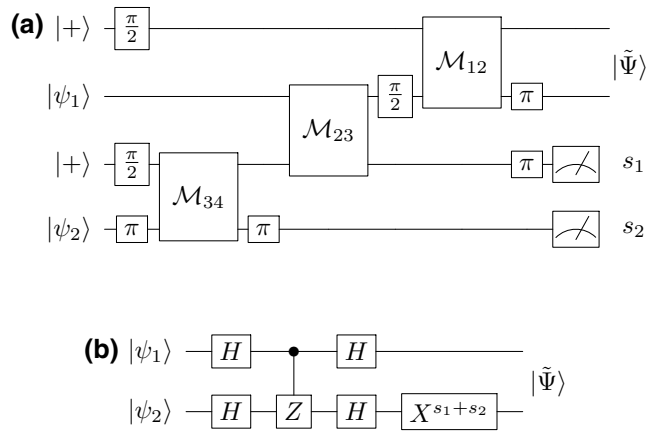


FIG. 7. (a) Circuit diagram of the phase gates (π or $\pi/2$) and measurement sequence needed to achieve a two-qubit entangling unitary with two ancilla qubits. (b) Circuit diagram of the two-qubit unitary performed by the measurement and phase sequence given in (a) with single Pauli- x correction.

implemented; however, non-Clifford two-qubit gates are possible with the same tools.

For the single-qubit gate scheme, the entangling measurement with the measurement on the ancilla qubit does not allow for leakage of the logical qubit, regardless of the phase gates used or the ancilla qubit's initial state. The two-qubit gate example given also suppresses leakage; however, this is due to the selection of the phase gates, initial ancilla states, and measurement sequence and is therefore a significant factor to consider when designing gates within this scheme. The gate times of both the single- and two-qubit gates are limited by the single-qubit phase gates. Assuming an exchange coupling of $J = 160$ MHz [26], gate times of approximately 80 ns for the Hadamard and approximately 140 ns for the rotated CZ gates are shown in Figs. 6 and 7, respectively.

This scheme offers a hybrid exchange-measurement-based approach to quantum computation similar to a traditional gate-based approach without the need for magnetic field gradients or driving fields and can be made to be robust to leakage as well as operated at the SOP of the physical qubits. The main limitation is the need for ancilla qubits initialized to the $|+\rangle$ state, as this method offers no way of preparing such states from a $|0\rangle$ or $|1\rangle$ state. Such states can be initialized by adiabatically turning off the exchange interaction [52,53] of a qubit in the triplet state, which is within the control parameters of the scheme. Unfortunately, however, since this scheme is more akin to traditional gate-based approaches to quantum computations, the inherent capability of the scheme with stabilizer codes described in Sec. III E does not apply to this scheme.

V. MEASUREMENT METHODS

In this work two schemes for MBQC with singlet-triplet spin qubits are given assuming only measurement of the singlet-triplet basis. This can be achieved in a number of different ways; however, here we consider two such methods. The conventional spin-to-charge method and the QND curvature method.

The conventional spin-to-charge method of measuring in the singlet-triplet is achieved by adiabatically tuning the tunnel coupling between the two dots being measured. Because of Pauli exclusion, the singlet state allows for hopping from $(1, 1)$ to $(0, 2)$, while the triplet state does not couple to the doubly occupied state [18]. If the singlet state is measured, it can then be reinitialized back to the $(1, 1)$ singlet state by again adiabatically tuning the tunnel coupling.

Alternatively, the singlet-triplet basis can be measured by coupling to a superconducting (SC) resonator [49]. The resonator is driven with frequencies $\omega_m \approx \omega_r$ and $\omega_s \approx \omega_q$ with strength ϵ_s , where ω_r is the frequency of the resonator, ω_m is the frequency of an external gate modulation near the resonator, and ω_q is the singlet-triplet qubit frequency. This

scheme exploits the quantum curvature of the qubits and is described as follows in the rotating frame and qubit-space of qubit-qubit interaction Hamiltonian (3):

$$\begin{aligned} H_{\text{meas}} = & (\omega_r - \omega_m)a^\dagger a + \frac{\omega_q - \omega_s}{2}\sigma_z \\ & + (\chi + \delta\omega)a^\dagger a\sigma_z + \frac{1}{2}(g_{\parallel}\sigma_z + g_0\sigma_0)(a + a^\dagger) \\ & + \epsilon_d(ae^{-i\omega_m t} + a^\dagger e^{i\omega_m t}). \end{aligned} \quad (21)$$

Here a (a^\dagger) is the annihilation (creation) operator of the resonator, g_{\parallel} is the longitudinal coupling between resonator and qubit, and g_0 is the static coupling. The important term here for measuring the state of the qubit is the $\Delta\omega$ term. This term is the change in the SC resonator frequency due to the state of the qubit. This term is given by the quantum curvature of the eigenenergies of the qubit and is defined as

$$\delta\omega = \hbar\omega_r^2 \left(\frac{\eta}{e_0} \right)^2 \frac{\partial^2 G(V_m^0)}{\partial V_m^2}, \quad (22)$$

where ω_r is the resonator frequency, η is the dimensionless parameter for resonator inductance, and $G(V_m^0)$ is defined, assuming the singlet-triplet qubit Hamiltonian, as

$$\begin{aligned} H = & E_s |s\rangle \langle s| + E_{t_0} |t_0\rangle \langle t_0| \\ =: & G(V_m^0)\mathbb{I} + C(V_m^0)\sigma_z. \end{aligned} \quad (23)$$

Measuring $\delta\omega$ is assumed to quickly perform a projective measurement in the singlet-triplet spin basis when the cavity is driven.

VI. LEAKAGE PROTECTION

Supposing input states free of leakage, any leakage during the protocols, either by exchange or interqubit measurement, will be corrected for by projective single-qubit measurements in the $m_z = 0$ subspace of all ancillae qubits, in both protocols, provided negligible scattering of the total m_z of the all the entangled qubits. The only channel for leakage of the final state of the data qubit(s) after all the gate protocols considered here is measurement leakage.

Both methods of measurement can be used for the two MBQC protocols given here. One major difference between the two methods is inherent protection against leakage. In the curvature measurement scheme, the $m_z = \pm 1$ states are energetically separated from the cavity frequency by an external magnetic field; however, in the spin-to-charge method, measurement of a triplet state is not exclusive to the t_0 state, but a projection onto all triplet states. This allows for measurement-induced leakage. Fortunately for MBQC, the outcome of the measurements of these is only consequential to the Pauli-correction terms. Consequently, so long as valley excitations are avoided,

the measurement need may instead be replaced with initializing the qubit into the $(0, 2)$ singlet state by decay or by varying the qubit detuning. For MBQC to function, the measured ancillae need to be completely removed from the entangled system, which in the case of singlet-triplet qubits means the two spins of the measured qubit be maximally entangled. Since projection onto a combination of all triplet states considered here does not completely remove the entangled qubit from the system, the measurement is in a sense incomplete. However, since the measurement is incomplete, the leakage due to the measurement is addressable. For example, in the first protocol, for a single-qubit rotation by measurement given in Eq. (9), suppose that the measurement of the ancilla is done by spin to charge and that the result is a triplet. After this measurement, the gate has not succeeded, but can be recovered by setting the detuning of the ancilla qubit back to the operating point and allowing the qubits to precess for time

$$\tau = \frac{4(\pi + 4\pi n)}{\sqrt{J_{23}^2 + 4\Delta_{23}^2 - 4\Delta_{23}}}, \quad (24)$$

where $n \in \mathbb{Z}$, then measuring the qubit again. Note that during this step it is assumed that the interqubit exchange $J_{23} = 0$; the term \tilde{J}_{23} is the exchange used in the previous pulse before the failed triplet measurement. The result of the following measurement must be a singlet, i.e., the measurement will be successful, and the only difference between the resulting rotation and the intended rotation is an additional Pauli- z correction term.

VII. DISCUSSION

Here protocols for full measurement-based qubit control with Si DQD qubits using two hybrid measurement-exchange schemes are given. The first protocol is given by entangling neighboring qubits with an exchange interaction and single-qubit measurements resulting in a spin-qubit cluster state approach to MBQC. This allows for full single- and two-qubit control with known Pauli and phase corrections. The leakage limitations of interqubit exchange gates do not apply to this protocol given projective single-qubit measurements without leakage, or by the correction steps given in Sec. V. This scheme is shown to also be useful for efficient arbitrary qubit state preparation. The nature of the measurements allows for the limiting of the required qubit resource overhead by recycling measured qubits back into the resource state with additional known required Pauli corrections. This allows for simple processor architectures designed for the arbitrary manipulation as well as encoding and decoding of a qubit state into a stabilizer state with five physical qubits in a 1D geometry.

A second protocol with entangling measurements is also shown by measuring in the singlet-triplet basis between one dot from one qubit with one dot from a different qubit.

This measurement-based protocol is closer to a traditional gate-based protocol, and can be made to be robust against leakage and can be operated at the SOP of all the physical qubits, requiring only measurements and phase gates. Again, although the entangling measurements couple to states outside of the qubit subspace, single-qubit measurements limited to qubit subspace will remove all leakage from the end result of each gate.

In the first protocol, a single single-qubit gate consists of one exchange gate and one measurement, whilst a two-qubit control consists of four exchange gates and two measurements, all performed simultaneously, assuming measurement by curvature. In the second protocol single-qubit gates consist of three exchange gates and two measurements, whilst two-qubit gates consist of seven exchange gates, five measurements, and n ancilla qubits per n data qubits (total $2n$ physical qubits), again assuming measurement by curvature. The first proposed protocol is an improvement compared to conventional gate-based leakage resistant schemes in singlet-triplet encoded qubits with magnetic field gradients, where single-qubit leakage errors can be corrected with a minimum of five exchange gates and one ancilla qubit [54], and two-qubit gates are assumed to be given by long-range cavity coupling, unlike in the work presented. Additionally, the second

TABLE I. Table comparing the number of exchange gates, timesteps, measurements, ancillae between the first proposed cluster state protocol, and leakage-protected operations in singlet-triplet qubits with magnetic field gradients from the literature [54], and the second entangling measurements protocol and gradient-free exchange-only three-spin-encoded qubits from the literature [55]. Single-qubit operations from the literature are not robust to leakage, so the given numbers include leakage correction circuits after a rotation. There are no two-qubit leakage robust sequences in the literature, only leakage suppressed, so for comparison, the leakage correction circuit is considered twice. Both proposed protocols offer significant improvements over their similar respective counterparts.

	Protocol 1	S/T_0	Protocol 2	Three spin
Single-qubit gate				
Gates	1	1	3	4
Measurements	1	...	2	...
Ancillae	1	0	1	0
Leakage protected	Yes	No	Yes	No
Correction gates	...	7	...	30
Correction ancillae	...	1	...	1
Two-qubit gate				
Gates	4	1	7	22
Measurements	2	...	5	...
Ancillae	2	0	2	0
Leakage protected	Yes	No	Yes	Yes
Correction gates	...	14
Correction ancillae	...	2

proposed protocol is more efficient than leakage protection and correction in similar systems without magnetic field gradients, three-spin exchange-only qubits. In such systems, active leakage reduction requires 30 exchange gates and protected two-qubit gates require a minimum of 22 exchange gates [55], which can be improved by chip geometry or with dynamic gates [56,57]. A direct comparison of these schemes is made in Table I. Equally, both schemes are superior when compared to superconducting systems that can also experience leakage errors, requiring 16 single- and two-qubit gates and two measurements [58].

This work promises alternative hybrid exchange-measurement-based quantum computation schemes. The estimated gate times for all the schemes proposed here are < 150 ns and so are all well within expected relaxation times of Si DQD spin qubits of tens of microseconds [59]. This allows for semiconductor qubits to take advantage of MBQC without the resource overhead or necessity for arbitrary rotated measurement schemes, and with the addition of control by exchange, allows for more deterministic control compared to other proposals [39].

ACKNOWLEDGMENTS

We acknowledge helpful discussions with M. Benito, R. Ruskov, M. Russ, YP. Shim, V. Shkolnikov, and Y. Yanay.

- [1] Robert Raussendorf and Hans J. Briegel, Quantum computing via measurements only, arXiv preprint [ArXiv:quant-ph/0010033](https://arxiv.org/abs/quant-ph/0010033) (2000).
- [2] Frank Verstraete and J. Ignacio Cirac, Valence-bond states for quantum computation, *Phys. Rev. A* **70**, 060302 (2004).
- [3] Robert Raussendorf, Daniel Browne, and Hans Briegel, The one-way quantum computer—a non-network model of quantum computation, *J. Mod. Opt.* **49**, 1299 (2002).
- [4] M. A. Nielsen, Universal quantum computation using only projective measurement, quantum memory, and preparation of the 0 state, arXiv preprint [ArXiv:quant-ph/0108020](https://arxiv.org/abs/quant-ph/0108020) (2001).
- [5] Robert Raussendorf, Measurement-based quantum computation with cluster states, *Int. J. Quantum Inf.* **7**, 1053 (2009).
- [6] Richard Jozsa, An introduction to measurement based quantum computation, NATO science series, III: Computer and systems sciences., Quantum Inf. Proc.-From Theory Exp. **199**, 137 (2006).
- [7] Dan Browne and Hans Briegel, in *Quantum Information* (John Wiley & Sons, Ltd, 2019), Chap. 21, p. 449.
- [8] Robert Raussendorf and Jim Harrington, Fault-Tolerant Quantum Computation with High Threshold in two Dimensions, *Phys. Rev. Lett.* **98**, 190504 (2007).
- [9] Maarten Van den Nest, Akimasa Miyake, Wolfgang Dür, and Hans J. Briegel, Universal Resources for Measurement-Based Quantum Computation, *Phys. Rev. Lett.* **97**, 150504 (2006).

- [10] A. Douglas K. Plato, Oscar C. Dahlsten, and Martin B. Plenio, Random circuits by measurements on weighted graph states, *Phys. Rev. A* **78**, 042332 (2008).
- [11] Nathan Shettell and Damian Markham, Graph States as a Resource for Quantum Metrology, *Phys. Rev. Lett.* **124**, 110502 (2020).
- [12] Rami Barends, Julian Kelly, Anthony Megrant, Andrzej Veitia, Daniel Sank, Evan Jeffrey, Ted C. White, Josh Mutus, Austin G. Fowler, and Brooks Campbell, *et al.*, Superconducting quantum circuits at the surface code threshold for fault tolerance, *Nature* **508**, 500 (2014).
- [13] Frank Arute, Kunal Arya, Ryan Babbush, Dave Bacon, Joseph C. Bardin, Rami Barends, Rupak Biswas, Sergio Boixo, Fernando G.S.L. Brandao, and David A. Buell, *et al.*, Quantum supremacy using a programmable superconducting processor, *Nature* **574**, 505 (2019).
- [14] John Preskill, Quantum computing in the nisq era and beyond, *Quantum* **2**, 79 (2018).
- [15] Yuanhao Wang, Ying Li, Zhang-qi Yin, and Bei Zeng, 16-qubit ibm universal quantum computer can be fully entangled, *npj Quantum Inf.* **4**, 1 (2018).
- [16] Jiehang Zhang, Guido Pagano, Paul W. Hess, Antonis Kyprianidis, Patrick Becker, Harvey Kaplan, Alexey V. Gorshkov, Z.-X. Gong, and Christopher Monroe, Observation of a many-body dynamical phase transition with a 53-qubit quantum simulator, *Nature* **551**, 601 (2017).
- [17] C. J. Ballance, T. P. Harty, N. M. Linke, M. A. Sepiol, and D. M. Lucas, High-Fidelity Quantum Logic Gates Using Trapped-Ion Hyperfine Qubits, *Phys. Rev. Lett.* **117**, 060504 (2016).
- [18] Ronald Hanson, Leo P. Kouwenhoven, Jason R. Petta, Seigo Tarucha, and Lieven M. K. Vandersypen, Spins in few-electron quantum dots, *Rev. Mod. Phys.* **79**, 1217 (2007).
- [19] Maximilian Russ and Guido Burkard, Three-electron spin qubits, *J. Phys.: Condens. Matter* **29**, 393001 (2017).
- [20] Xiao Mi, Mónica Benito, Stefan Putz, David M. Zajac, Jacob M. Taylor, Guido Burkard, and Jason R. Petta, A coherent spin–photon interface in silicon, *Nature* **555**, 599 (2018).
- [21] M. Veldhorst, H. G. J. Eeenink, C. H. Yang, and Andrew S. Dzurak, Silicon CMOS architecture for a spin-based quantum computer, *Nat. Commun.* **8**, 1 (2017).
- [22] Kenta Takeda, Akito Noiri, Jun Yoneda, Takashi Nakajima, and Seigo Tarucha, Resonantly Driven Singlet-Triplet Spin Qubit in Silicon, *Phys. Rev. Lett.* **124**, 117701 (2020).
- [23] C. H. Yang, K. W. Chan, R. Harper, W. Huang, T. Evans, J. C. C. Hwang, B. Hensen, A. Laucht, T. Tanttu, and F. E. Hudson, *et al.*, Silicon qubit fidelities approaching incoherent noise limits via pulse engineering, *Nat. Electron.* **2**, 151 (2019).
- [24] David M. Zajac, Anthony J. Sigillito, Maximilian Russ, Felix Borjans, Jacob M. Taylor, Guido Burkard, and Jason R. Petta, Resonantly driven cnot gate for electron spins, *Science* **359**, 439 (2018).
- [25] Maximilian Russ, David M. Zajac, Anthony J. Sigillito, Felix Borjans, Jacob M. Taylor, Jason R. Petta, and Guido Burkard, High-fidelity quantum gates in si/sige double quantum dots, *Phys. Rev. B* **97**, 085421 (2018).
- [26] M. D. Reed, B. M. Maune, R. W. Andrews, M. G. Borselli, K. Eng, M. P. Jura, A. A. Kiselev, T. D. Ladd, S. T. Merkel,

- and I. Milosavljevic, *et al.*, Reduced Sensitivity to Charge Noise in Semiconductor Spin Qubits via Symmetric Operation, *Phys. Rev. Lett.* **116**, 110402 (2016).
- [27] Jun Yoneda, Kenta Takeda, Tomohiro Otsuka, Takashi Nakajima, Matthieu R. Delbecq, Giles Allison, Takumu Honda, Tetsuo Kodera, Shunri Oda, and Yusuke Hoshi, *et al.*, A quantum-dot spin qubit with coherence limited by charge noise and fidelity higher than 99.9%, *Nat. Nanotechnol.* **13**, 102 (2018).
- [28] Jeremy Levy, Universal Quantum Computation with spin-1/2 Pairs and Heisenberg Exchange, *Phys. Rev. Lett.* **89**, 147902 (2002).
- [29] A. C. Johnson, J. R. Petta, J. M. Taylor, A. Yacoby, M. D. Lukin, C. M. Marcus, M. P. Hanson, and A. C. Gossard, Triplet-singlet spin relaxation via nuclei in a double quantum dot, *Nature* **435**, 925 (2005).
- [30] Edward A. Laird, Jacob Mason Taylor, David P. DiVincenzo, Charles Masamed Marcus, Micah P. Hanson, and Arthur C. Gossard, Coherent spin manipulation in an exchange-only qubit, *Phys. Rev. B* **82**, 075403 (2010).
- [31] Matthew P. Wardrop and Andrew C. Doherty, Exchange-based two-qubit gate for singlet-triplet qubits, *Phys. Rev. B* **90**, 045418 (2014).
- [32] Reed W. Andrews, Cody Jones, Matthew D. Reed, Aaron M. Jones, Sieu D. Ha, Michael P. Jura, Joseph Kerckhoff, Mark Levendorf, Séan Meenehan, and Seth T. Merkel, *et al.*, Quantifying error and leakage in an encoded si/sige triple-dot qubit, *Nat. Nanotechnol.* **14**, 747 (2019).
- [33] Robert Raussendorf, Jim Harrington, and Kovid Goyal, A fault-tolerant one-way quantum computer, *Ann. Phys.* **321**, 2242 (2006).
- [34] B. A. Bell, D. A. Herrera-Martí, M. S. Tame, Damian Markham, W. J. Wadsworth, and J. G. Rarity, Experimental demonstration of a graph state quantum error-correction code, *Nat. Commun.* **5**, 1 (2014).
- [35] Antonio Russo, Edwin Barnes, and Sophia E. Economou, Photonic graph state generation from quantum dots and color centers for quantum communications, *Phys. Rev. B* **98**, 085303 (2018).
- [36] T. P. Bodiya and L.-M. Duan, Scalable Generation of Graph-State Entanglement through Realistic Linear Optics, *Phys. Rev. Lett.* **97**, 143601 (2006).
- [37] B. P. Lanyon, P. Jurcevic, M. Zwerger, C. Hempel, E. A. Martinez, W. Dür, H. J. Briegel, Rainer Blatt, and Christian F. Roos, Measurement-Based Quantum Computation with Trapped Ions, *Phys. Rev. Lett.* **111**, 210501 (2013).
- [38] Simon C. Benjamin, Brendon W. Lovett, and Jason M. Smith, Prospects for measurement-based quantum computing with solid state spins, *Laser Photonics Rev.* **3**, 556 (2009).
- [39] Michael H. Freedman, Matthew B. Hastings, and Modjtaba Shokrian Zini, Symmetry protected quantum computation, arXiv preprint [ArXiv:2105.04649](https://arxiv.org/abs/2105.04649) (2021).
- [40] Torsten Karzig, Christina Knapp, Roman M. Lutchyn, Parsa Bonderson, Matthew B. Hastings, Chetan Nayak, Jason Alicea, Karsten Flensberg, Stephan Plugge, and Yuval Oreg, *et al.*, Scalable designs for quasiparticle-poisoning-protected topological quantum computation with majorana zero modes, *Phys. Rev. B* **95**, 235305 (2017).
- [41] Zheng-Yuan Xue, Measurement based controlled not gate for topological qubits in a majorana fermion and quantum-dot hybrid system, *Eur. Phys. J. D* **67**, 89 (2013).
- [42] Parsa Bonderson and Roman M. Lutchyn, Topological Quantum Buses: Coherent Quantum Information Transfer between Topological and Conventional Qubits, *Phys. Rev. Lett.* **106**, 130505 (2011).
- [43] Arne L. Grimsmo and Thomas B. Smith, Majorana qubit readout using longitudinal qubit-resonator interaction, *Phys. Rev. B* **99**, 235420 (2019).
- [44] Floris A. Zwanenburg, Andrew S. Dzurak, Andrea Morello, Michelle Y. Simmons, Lloyd C. L. Hollenberg, Gerhard Klimeck, Sven Rogge, Susan N. Coppersmith, and Mark A. Eriksson, Silicon quantum electronics, *Rev. Mod. Phys.* **85**, 961 (2013).
- [45] Robert P. G. McNeil, R. Jeff Schneble, Masaya Kataoka, Christopher J. B. Ford, Takeshi Kasama, Rafal E. Dunin-Borkowski, Joshua M. Feinberg, Richard J. Harrison, Crispin H. W. Barnes, and Desmond H. Y. Tse, *et al.*, Localized magnetic fields in arbitrary directions using patterned nanomagnets, *Nano Lett.* **10**, 1549 (2010).
- [46] Rusko Ruskov, Menno Veldhorst, Andrew S. Dzurak, and Charles Tahan, Electron g-factor of valley states in realistic silicon quantum dots, *Phys. Rev. B* **98**, 245424 (2018).
- [47] Patrick Harvey-Collard, N. Tobias Jacobson, Chloé Bureau-Oxton, Ryan M. Jock, Vanita Srinivasa, Andrew M. Mounce, Daniel R. Ward, John M. Anderson, Ronald P. Manginell, and Joel R. Wendt, *et al.*, Spin-Orbit Interactions for Singlet-Triplet Qubits in Silicon, *Phys. Rev. Lett.* **122**, 217702 (2019).
- [48] John S. Van Dyke, Yadav P. Kandel, Haifeng Qiao, John M. Nichol, Sophia E. Economou, and Edwin Barnes, Protecting quantum information in quantum dot spin chains by driving exchange interactions periodically, *Phys. Rev. B* **103**, 245303 (2021).
- [49] Rusko Ruskov and Charles Tahan, Quantum-limited measurement of spin qubits via curvature couplings to a cavity, *Phys. Rev. B* **99**, 245306 (2019).
- [50] B. A. Bell, D. A. Herrera-Martí, M. S. Tame, D. Markham, W. J. Wadsworth, and J. G. Rarity, Experimental demonstration of a graph state quantum error-correction code, *Nat. Comms.* **5**, 3658 (2014). [ArXiv:1404.5498](https://arxiv.org/abs/1404.5498).
- [51] Rui Li, Xuedong Hu, and J. Q. You, Controllable exchange coupling between two singlet-triplet qubits, *Phys. Rev. B* **86**, 205306 (2012).
- [52] Sandra Foletti, Hendrik Bluhm, Diana Mahalu, Vladimir Umansky, and Amir Yacoby, Universal quantum control of two-electron spin quantum bits using dynamic nuclear polarization, *Nat. Phys.* **5**, 903 (2009).
- [53] M. A. Fogarty, K. W. Chan, B. Hensen, W. Huang, T. Tanttu, C. H. Yang, A. Laucht, M. Veldhorst, F. E. Hudson, and Kohei M. Itoh, *et al.*, Integrated silicon qubit platform with single-spin addressability, exchange control and single-shot singlet-triplet readout, *Nat. Commun.* **9**, 1 (2018).

- [54] Sebastian Mehl, Hendrik Bluhm, and David P. DiVincenzo, Fault-tolerant quantum computation for singlet-triplet qubits with leakage errors, *Phys. Rev. B* **91**, 085419 (2015).
- [55] Bryan H. Fong and Stephen M. Wandzura, Universal quantum computation and leakage reduction in the 3-qubit decoherence free subsystem, arXiv preprint [ArXiv:1102.2909](https://arxiv.org/abs/1102.2909) (2011).
- [56] F. Setiawan, Hoi-Yin Hui, J. P. Kestner, Xin Wang, and S. Das Sarma, Robust two-qubit gates for exchange-coupled qubits, *Phys. Rev. B* **89**, 085314 (2014).
- [57] G. T. Hickman, Xin Wang, J. P. Kestner, and S. Das Sarma, Dynamically corrected gates for an exchange-only qubit, *Phys. Rev. B* **88**, 161303 (2013).
- [58] Joydip Ghosh and Austin G. Fowler, Leakage-resilient approach to fault-tolerant quantum computing with superconducting elements, *Phys. Rev. A* **91**, 020302 (2015).
- [59] A. J. Sigillito, J. C. Loy, D. M. Zajac, M. J. Gullans, L. F. Edge, and J. R. Petta, Site-Selective Quantum Control in an Isotopically Enriched si 28/si 0.7 ge 0.3 Quadruple Quantum dot, *Phys. Rev. Appl.* **11**, 061006 (2019).